UCLA
UCLA Previously Published Works

Title

A 500-Year Tree Ring-Based Reconstruction of Extreme Cold-Season Precipitation and Number of Atmospheric River Landfalls Across the Southwestern United States

Permalink

https://escholarship.org/uc/item/1tk8624d

Journal

Geophysical Research Letters, 45(11)

ISSN

0094-8276

Authors

Steinschneider, Scott
Ho, Michelle
Williams, A Park
et al.

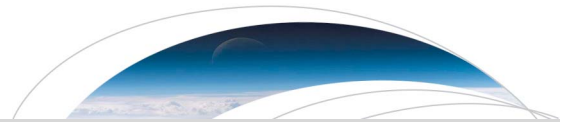**Publication Date**

2018-06-16

DOI

10.1029/2018gl078089

Peer reviewed

RESEARCH LETTER

Key Points:
- The first two EOFs of a reconstructed drought index in the southwestern Unites States relate to two major atmospheric river storm tracks over the region
- A network of tree ring chronologies in the Southwest can accurately reconstruct landfalling atmospheric rivers along the southwest coast
- The network of chronologies can also reconstruct the occurrence of extreme precipitation along the southern California coastline

Supporting Information:
- Supporting Information S1

Correspondence to:
S. Steinschneider,
ss3378@cornell.edu

A 500-Year Tree Ring-Based Reconstruction of Extreme Cold-Season Precipitation and Number of Atmospheric River Landfalls Across the Southwestern United States

Scott Steinschneider[1] (iD), Michelle Ho[2] (iD), A. Park Williams[3] (iD), Edward R. Cook[3] (iD), and Upmanu Lall[2] (iD)

[1]Department of Biological and Environmental Engineering, Cornell University, Ithaca, NY, USA, [2]Department of Earth and Environmental Engineering, Columbia University, New York, NY, USA, [3]Tree Ring Lab, Lamont-Doherty Earth Observatory, Palisades, NY, USA

Abstract This study develops a reconstruction of the frequency of extreme cold-season precipitation and the occurrence of landfalling atmospheric river (AR) storm tracks across the southwestern Unites States using a network of tree ring chronologies and the Living Blended Drought Atlas (LBDA), a 500-year tree ring based reconstruction of the summer Palmer Drought Severity Index. The first two rotated empirical orthogonal functions of the LBDA across the Southwest are shown to relate well to previously identified patterns of regional AR activity. Accordingly, the rotated empirical orthogonal functions also record patterns of extreme precipitation associated with those ARs, albeit with some uncertainty introduced by nonextreme precipitation. A network of chronologies sensitive to cold-season precipitation is then used to reconstruct the occurrence of landfalling ARs and extreme precipitation along the southern Californian coast, demonstrating for the first time the feasibility of reconstructing AR landfalls and extreme events in the Southwest based on spatial patterns in a network of dendroclimatic proxies.

Plain Language Summary Extreme precipitation and flood events are a significant hazard to society. Along the West Coast, many of these extreme events are linked to a particular type of storm called an atmospheric river. Intense atmospheric rivers that make landfall are rare, and this makes it difficult to assess the likelihood of these storms and whether this likelihood is changing over time. In this study, we present the first attempt to predict the occurrence of landfalling atmospheric rivers impacting the southwest coast of the Unites States over the past 500 years, as well as extreme precipitation associated with these storms. To do this, we use a series of tree ring chronologies that record winter precipitation amounts in the widths of tree rings, which for some trees can extend backward in time for hundreds of years. Because intense atmospheric rivers bring substantial precipitation amounts that extend far into the interior of the western Unites States, we show that a network of tree ring chronologies across this region can predict when atmospheric rivers made landfall along the coast. This enables a better understanding of past variability in these storms, which can be used to contextualize observed trends or predicted changes in storm frequency under anthropogenic climate change.

1. Introduction

Along much of the western coast of the Unites States, precipitation primarily accumulates over the cold season (October–March) and is driven by synoptic-scale cyclones originating over the Pacific Ocean. Some of these cyclones are associated with atmospheric rivers (ARs), filamentary organizational processes that transport substantial amounts of moisture from the subtropical and tropical oceans toward the coastline, which then precipitates out under orographic lift along the Peninsular, Sierra Nevada, and Cascade ranges (Zhu & Newell, 1994). ARs are a major societal hazard in the region linked to extreme precipitation and severe flooding (Dettinger, 2004; Ralph et al., 2006). They are also a critical source of water supply, particularly in the Mediterranean and semiarid regions of central and southern California, where they are estimated to deliver between 30 and 50% of the total precipitation (Dettinger, 2013; Dettinger et al., 2011; Guan et al., 2010).

While much of the moisture associated with ARs is removed on the western side of mountain ranges near the coast of western North America, these storms can deliver moisture further inland. ARs have recently been identified as an important source of water supply and a driver of extreme events during the cold season in the semiarid U.S. Intermountain West (defined as the region between the Peninsular, Sierra Nevada, and

Cascade ranges on the west and Rockies on the east; Rutz & Steenburgh, 2012). In the Southwest, ARs that penetrate the Peninsular Range running along southern California and the Baja Peninsula have been associated with extreme floods in major watersheds like the Verde and Salt River Basins (Demaria et al., 2017; Hughes et al., 2014; Neiman et al., 2013). Rivera et al. (2014) identified two primary storm tracks among days when ARs hit the Verde Basin: (1) a zonally oriented track that originates far to the west near Hawaii and is associated with a midlevel offshore trough west of central California and (2) a shorter, meridional track associated with a midlevel cutoff low over the Pacific off the west coast of the Baja Peninsula. Similar storm tracks were also identified by Rutz et al. (2014, 2015) and Alexander et al. (2015) as part of a larger typology of preferential pathways for ARs that penetrate into the Intermountain West. These studies showed that substantial water vapor depletion over major topographic barriers (e.g., the High Sierra) cause ARs to rapidly decay from the coastline, but conduits of milder terrain can funnel ARs further into the continental interior. These fixed orographic conduits vary latitudinally within gaps in the Cascades, Sierra Nevada, and Peninsular Ranges and influence the proportion of ARs that penetrate into the Intermountain West and their path over land.

The tendency of ARs to penetrate into the continental interior is related to their wind speed and moisture content (Rutz et al., 2015). Intense ARs that are more prone to cause large-scale extreme precipitation along the western U.S. coast are also likely to penetrate into the Intermountain West. In this study, we examine whether the large network of tree ring chronologies along the West Coast and across the Intermountain West can inform us as to the frequency of incidence of ARs and associated extreme precipitation. This study builds on past work that has shown that tree ring chronologies can be used to reconstruct the occurrence of and gradients in precipitation in the Southwest and California (Meko et al., 2011; Woodhouse & Meko, 1997), as well as pressure patterns and storm tracks in the Pacific Northwest (Wise & Dannenberg, 2014, 2017). Here we contribute a more focused examination on extreme precipitation and associated ARs. We recognize that persistent, moderate precipitation delivered from weaker extratropical cyclones can contribute substantially to seasonal rainfall, especially in years where ARs are not active, and hence, extreme precipitation events are limited. However, recently, we found that the potential to link extreme precipitation to a tree ring-based reconstruction of the summer Palmer Drought Severity Index (PDSI) is high in the Southwest (Steinschneider et al., 2016). Annual tree growth increments are highly responsive to moisture from extreme winter precipitation through subsequent snowmelt during the growing season in this region (St. George & Ault, 2014; Williams et al., 2010; Woodhouse & Meko, 1997) but are relatively insensitive to summer precipitation associated with the North American Monsoon due to high rates of evaporation (St. George et al., 2010). Therefore, we maintain a regional focus on the Southwest in this work.

We find that the two primary modes of variability in a gridded, 500-year tree ring-based reconstruction of the summer PDSI across the southwestern Unites States are associated with the two primary AR storm track patterns over the region, as identified by Rivera et al. (2014) and confirmed in later work (Alexander et al., 2015; Rutz et al., 2014, 2015; Swales et al., 2016). We also find that the two modes of variability in tree ring-based moisture relate to the occurrence of extreme precipitation in the region, particularly in areas along the southern California coast and in southwest Arizona. We use a generalized linear regression directly on a network of chronologies sensitive to cold-season moisture across the West Coast and the Intermountain West to reconstruct the variability of AR landfalls along the southern California coastline, as well as extreme precipitation occurrences and amounts on the West Coast near Los Angeles. The reconstructions accurately reproduce the variability in AR landfalls and extreme precipitation occurrences during the instrumental record, with significant but weaker regression results on the average magnitude of extreme precipitation amounts. The reconstructions also align well with documented extreme events in the nineteenth century. To our knowledge, this is the first attempt to reconstruct the occurrence of storm tracks and associated extreme precipitation events in the southwestern Unites States based on a network of tree ring chronologies.

## 2. Relating Rotated EOFs of Tree Ring-Based Moisture to Southwest ARs

The first part of the analysis is based on the Living Blended Drought Atlas (LBDA; Cook et al., 2010), which is the latest update of the North American Drought Atlas (Cook et al., 1999) and provides a reconstruction of the summer PDSI from 1451 to 2005 based on a point-by-point regression with tree ring chronologies within a 450 km search radius. We perform an empirical orthogonal function (EOF) analysis on the LBDA over the entire record across the West Coast and Intermountain West in a region west of 105°W between 23°N and
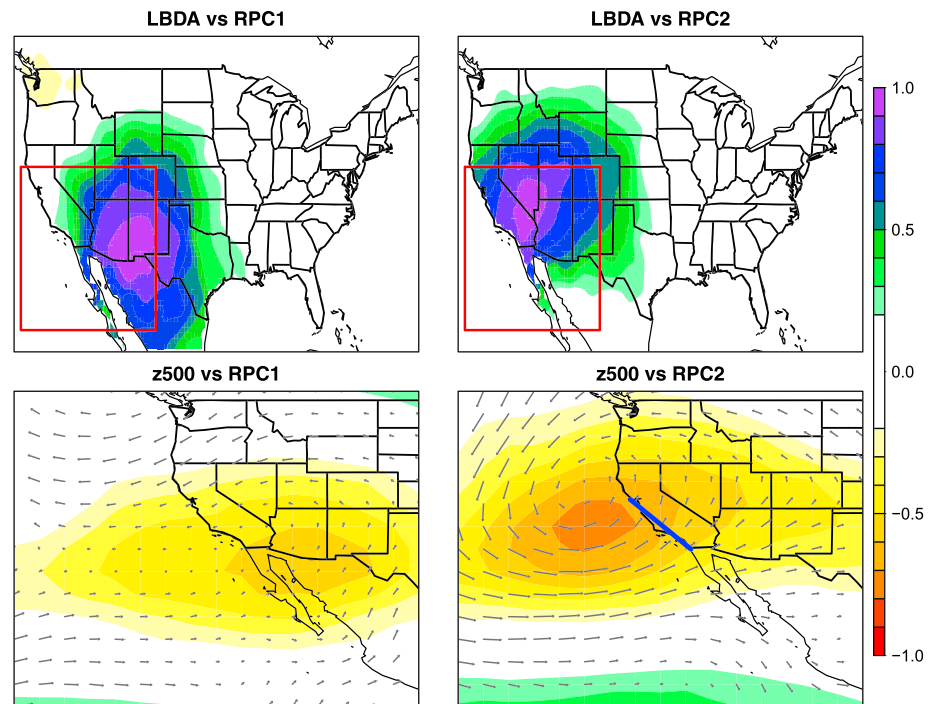
Figure 1. Spearman correlation between the RPCs of the first two rotated EOFs of (top) the Southwest LBDA (boxed region) and (top) the gridded LBDA across North America and (bottom) October–March average 500 hPa geopotential height anomalies. Composites of anomalous October–March integrated water vapor transport (IVT) for the years with the 20 largest RPC values are shown as arrows in the bottom figures (maximum IVT shown is 285 kg · m^{-1} · s^{-1}). A transect for counts of landfalling ARs is shown in blue.

40°N (hereafter referred to as the Southwest LBDA) and retain the first two EOFs (containing ~80% of the total variability) before applying a varimax rotation (Figures 1a and 1b). Within the defined region, the LBDA has been shown to relate strongly to winter precipitation, but has no significant relationship to summertime precipitation, allowing the winter signal to be isolated (St. George et al., 2010). The leading rotated component (RPC1) represents a north-south oriented footprint of moisture extending from central Mexico to southern Wyoming with a center located between southern Arizona and New Mexico. The second mode (RPC2) maintains a southwest-to-northeast orientation that extends from southwestern California to the western edge of the Rocky Mountains, with a primary lobe centered in southern California and Nevada. These spatial patterns are very consistent if the rotated EOF analysis is conducted over different 100-year periods of record, although the two modes can switch order (see Figure S1).

We correlate average cold-season (October–March) 500 hPa geopotential heights between 1949 and 2005 from the National Centers for Environmental Prediction/National Center for Atmospheric Research (NCEP/NCAR) Reanalysis I (2.5° by 2.5°; Kalnay et al., 1996) to the RPCs associated with the first two modes of the Southwest LBDA, and composite anomalous, cold-season integrated water vapor transport (IVT) from the same reanalysis data set for the years with the 20 largest values for each RPC. The first mode of the Southwest LBDA is related to a confined low-pressure center over Northwestern Mexico that drives a strong meridional IVT from the eastern subtropical Pacific through western Mexico and into the southwestern Unites States. This pattern resembles the second mode of IVT variability identified by Rivera et al. (2014), although the associated midlevel cutoff low and IVT are located further east over the Southwest. The second mode of the Southwest LBDA is associated with a broader trough off the California coast that drives a longer and zonally oriented flux of IVT from the central subtropical Pacific toward the southern California coastline. This pattern resembles the first mode of IVT variability identified by Rivera et al. (2014), although the trough and IVT are shifted further to the north. The differences from the results in Rivera et al. (2014) reflect the regional scale of our analysis and are similar to AR pathways identified in Rutz et al. (2015, their Figure 16), and suggest that the first two leading modes of variability in the Southwest LBDA record major modes of IVT variability that represent key AR typologies impacting the Southwest.
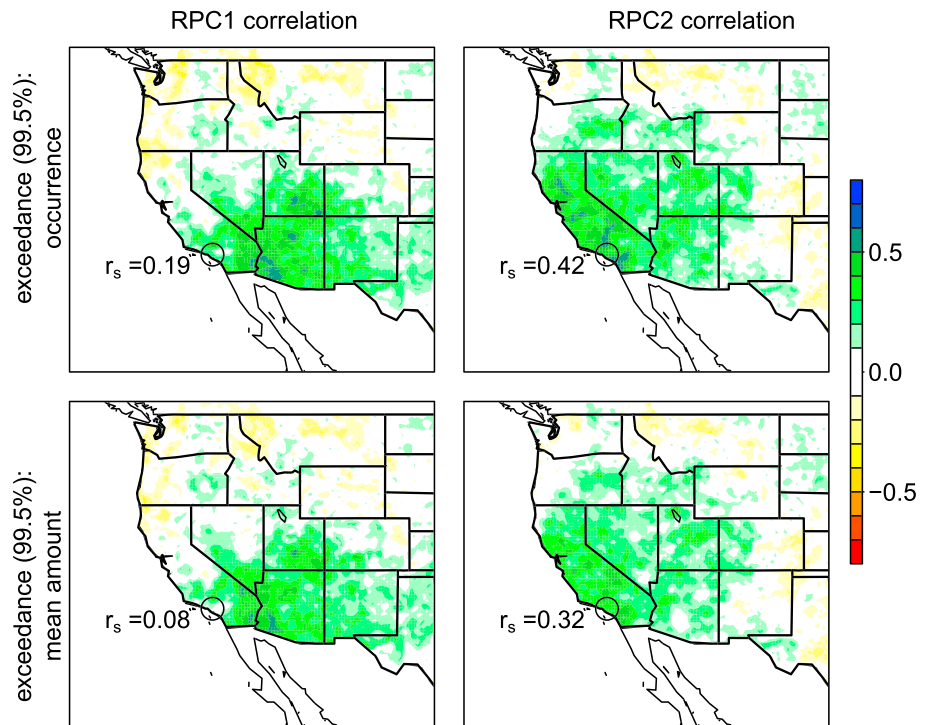
Figure 2. Spearman correlations between the (top) occurrence and (bottom) average magnitude of extreme daily precipitation events during the cold season (October–March) with (left) RPC1 and (right) RPC2 of the Southwest LBDA between 1949 and 2005. Correlation values near Los Angeles are highlighted.

The relationships in Figure 1 suggest that the leading modes of Southwest LBDA variability may also record information regarding the risk of extreme precipitation in the Southwest associated with landfalling ARs. Using the daily, gridded precipitation data set of Livneh et al. (2013), we calculate the number and average magnitude of extreme precipitation events in the cold season for each year, defined as any precipitation event that exceeds the 99.5th percentile (approximately two events per year on average). We correlate the occurrence and magnitude of extreme precipitation with both RPC1 and RPC2 of the Southwest LBDA (Figure 2). We find that RPC1 informs both the occurrence and average magnitude of extreme precipitation in a region centered in southwestern Arizona, while RPC2 is more strongly related to the occurrence and to a lesser extent the magnitude of extreme precipitation in southern California. Both patterns are consistent with the storm track orientations in Figure 1. Spearman correlation values upward of 0.6–0.65 are noted in certain regions of California and Arizona. Consistent with the results of Woodhouse and Meko (1997), the relationship is stronger with extreme precipitation occurrence than average magnitude, since the tree ring-based moisture proxy is likely more sensitive to the total precipitation delivered (which is well represented by the number of extremes) rather than resolving the average degree of wetness for any event.

Overall, the relationships in Figure 2 suggest the potential to reconstruct the risk of extreme precipitation occurrences and to a lesser degree its magnitude based on spatial patterns in the LBDA. However, even in the regions with strongest correlations, there are times when the RPCs are elevated but few if any extremes occurred (not shown), suggesting that the modes of the Southwest LBDA in these cases are being driven by less extreme precipitation. We explored how varying the threshold of extreme precipitation through the set of 85th, 90th, 95th, and 99th percentiles of daily precipitation values changes the correlation maps in Figure 2 (Figure S2). These maps show that an increasing amount of the variability in the occurrence of extreme precipitation can be explained by RPC1 and RPC2 as the threshold used to define extreme precipitation is relaxed, with Spearman correlation coefficients upward of 0.75 across a broad swath of the Southwest if the threshold is decreased to the 95th percentile (approximately 18 events per year). The variance explained ceases to change much once the threshold is reduced to between the 85th and 90th percentiles, which coincides with precipitation amounts near zero in the Southwest (i.e., total cold-season precipitation). Importantly though, the amount of variability explained for the average magnitude of extremes does not noticeably

improve as the threshold is relaxed, again indicating that the tree ring-based proxies may be better suited to identify the occurrence of extreme precipitation in the region.

3. Reconstruction of ARs and Extreme Rainfall in Southern California

The composites of IVT in Figure 1 and the relationships to extreme precipitation in Figure 2 suggest that information recorded by dendroclimatic proxies in southern California and extending toward the Rockies in Colorado is related to the landfall of ARs along the southwest coastline. Further, tree ring chronologies in Mexico and southern Arizona and New Mexico may be inversely related to the occurrence of ARs impacting the southern California coast, as the occurrence of the cutoff low associated with RPC1 may reduce the likelihood of the midlevel trough off the California coast associated with RPC2 in the same season. To explore the potential to reconstruct AR variability based on these findings, we collect occurrences of AR landfalls along the southern California coast (south of 38°N; see Figure 1) from the recent data set of Brands et al. (2017). ARs in this data set are defined based on IVT calculated over different periods from four reanalysis products: NCEP/NCAR Reanalysis 1 (NCEP/NCAR; Kalnay et al., 1996), National Oceanic and Atmospheric Administration (NOAA) Cooperative Institute for Research in Environmental Sciences (CIRES) twentieth-century reanalysis v2 (NOAA-20C; Compo et al., 2011), European Centre for Medium-Range Weather Forecasts (ECMWF) ERA-20C reanalysis (ERA-20C; Poli et al., 2013), and ECMWF ERA-interim reanalysis (ERA-Interim; Dee et al., 2011). The data set provides different AR landfall occurrences for different combinations of AR detection and tracking thresholds, enabling a sensitivity analysis based on the definition of ARs (see the supporting information for more details). For the three longer reanalysis products (NCEP/NCAR, NOAA-20C, and ERA-20C), we produce an annual time series of the frequency of ARs impacting the southern California coast each cold season for 1950–1990. We then conduct a Poisson regression to relate the occurrence of landfalling ARs directly to a network of chronologies that are sensitive to cold-season moisture across the West Coast and the Intermountain West. These chronologies, which most often extend to 1990, have been prescreened from the larger regional network to ensure that they only record significant variations in cold-season precipitation (Torbenson, 2018). A lasso penalty is applied in the regression for simultaneous model selection and fitting. Model fitting, evaluation, and uncertainty estimation are described in the supporting information. The final reconstruction of AR occurrences uses a nested set of three separate regressions based on different sets of chronologies due to the difference in chronology length over the 1451–1990 time period.

Figure 3a shows the rank correlation between each chronology and the number of AR landfall occurrences from the ERA-20C reanalysis. Other reanalysis products yielded similar results (Figure S3). As expected, many of the chronologies in southern and central California are well correlated with AR landfalls. However, similar to the pattern of RPC2 in Figure 1, there are also significant relationships with chronologies further into the Intermountain West, including in northwestern Arizona and western New Mexico and Colorado, indicating that the penetration of these ARs into the Intermountain West leaves a footprint of moisture along their path into the continental interior. AR landfalls are also significantly and inversely correlated to some chronologies in central Mexico, suggesting that rainfall in that region becomes less likely as the number of AR landfalls increase along the southwest California coastline. This could be because a persistent trough to the west of central California associated with a high number of AR landfalls along the coastline reduces the likelihood of a strong cutoff low over the Baja Peninsula linked to the meridional ARs associated with RPC1 in Figure 1. Chronologies in all of the regions mentioned above were selected by the final set of nested regressions (Figure S4), which fit the observed number of AR landfall occurrences during the instrumental period very well (Figure 3b) and provide between a 63–74% improvement over a stationary Poisson model (as determined by its deviance ratio, see the supporting information for more details). The reconstruction of AR landfalls (Figure 3c) also shows large increases during times of well-documented floods in southern and central California and parts of Arizona prior to the instrumental record used here (i.e., prior to 1950), including the Great Flood of 1862 and extending through a series of floods in southern California and Arizona in the late nineteenth and early twentieth centuries (e.g., 1868, 1890, 1891, 1906, 1907, 1909, 1916, and 1941; Dobyns, 1981; Paulson et al., 1989). The reconstruction also shows a notable decrease in AR landfalls in the second half of the 1400s and first half of the 1500s, which has been associated with increased drought activity in the Southwest (Cook et al., 2014), although a large peak in AR landfalls punctuates this period in the late 1400s. We note that the linear relationship found between AR landfall occurrences and chronologies, even during the largest flood events in the historical record, is likely associated with additional chronologies
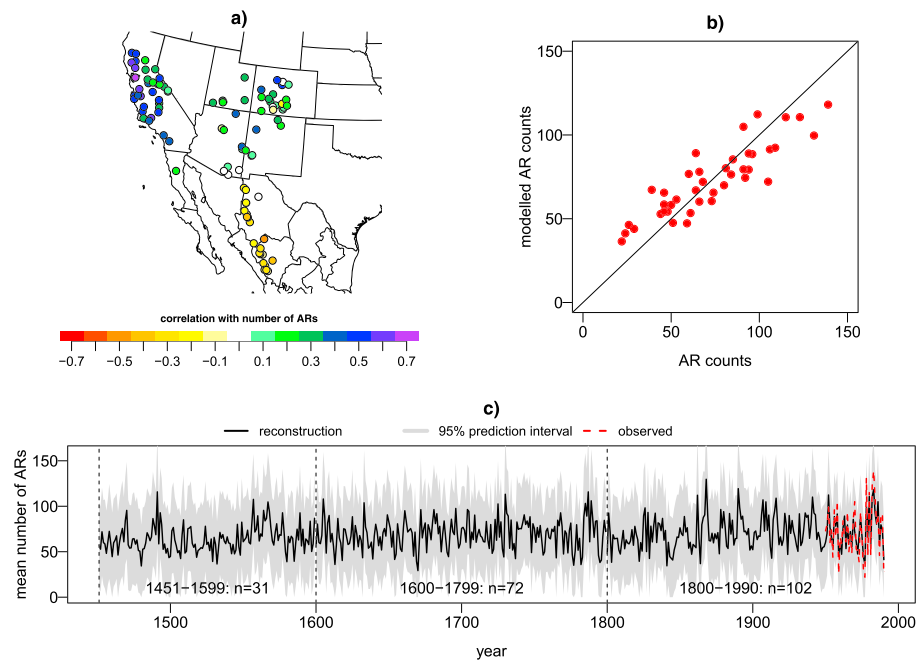
Figure 3. (a) Spearman correlation between number of landfalling ARs along the southern coast of California and cold-season chronologies between 1950 and 1990. (b) Observed versus predicted number of landfalling ARs from 1950 to 1990 based on a Poisson regression using a lasso penalty and 102 available chronologies. (c) Time series of observed (red) and reconstructed (black) AR landfall occurrences using a Poisson lasso regression, with 95% prediction interval.

recording a strong moisture signal over a wider region, since tree growth at any one location may not respond beyond some upper threshold of available moisture. Finally, we also examine the sensitivity of the above model to the definition of ARs based on different detection and tracking algorithms used in the Brands et al. (2017) data set. We find that lower IVT thresholds, particularly for AR detection, generally improve the relationship with AR landfall occurrences (Figure S5). This is consistent with the results in Figure S2 and suggests that the tree ring chronologies are better able to reconstruct the risk of all large storms, not just the most extreme.

The AR landfalls used above extend across a long stretch of California coastline and therefore could impact extreme precipitation and flooding in multiple areas, including central and southern California and parts of Arizona and New Mexico (see AR pathways in Rutz et al., 2015, their Figure 16). To create a more locally focused reconstruction of extremes, we perform a similar Poisson lasso regression against the occurrence of extreme precipitation events in Los Angeles based on the long precipitation record at the Los Angeles airport. We also perform a linear regression against the logarithm of the nonzero average magnitude of exceedances.

Similar to AR landfalls, the nested regression models for extreme precipitation occurrences also select chronologies in the Intermountain West for the final reconstruction (Figure S6). Again, this is consistent with the AR tracks associated with RPC2 that impact southern California and travel south of the High Sierra before extending further inland into southern Nevada and Utah. The nested regressions accurately explain the variability in the observed data (Figure 4a, also see Figure S7a), providing between a 50–60% improvement over a stationary Poisson model, and align well with historic records of past flood years in southern California (Figure 4c; Paulson et al., 1989). We note though that the reduction in variance of extreme precipitation occurrences prior to 1600 is an artifact of fewer available chronologies in that period. Thus, the magnitude of the reconstruction across time periods should be compared separately for each of the three nested regression models (see Figure S8).

The regression on extreme precipitation amounts is much less accurate than that for occurrences (Figure 4b; also see Figure S7b). Accordingly, we omit presenting the reconstruction of extreme precipitation amounts. The lack of skill again confirms that the tree ring chronologies are likely better suited to record the occurrence
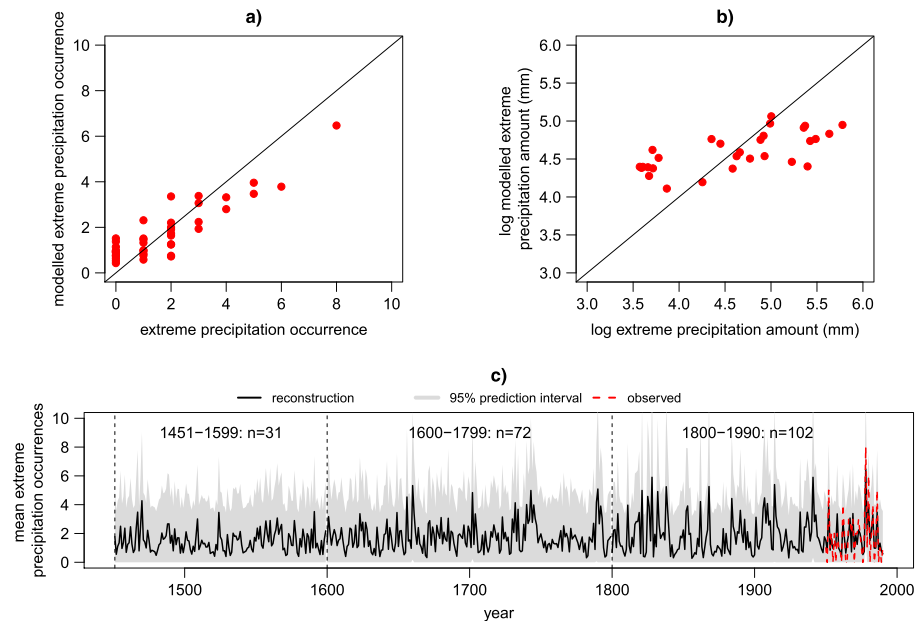
Figure 4. Observed versus predicted (a) number of extreme precipitation occurrences and (b) extreme precipitation amounts in Los Angeles between 1950 and 1990, based on a Poisson regression and linear regression on log transformed nonzero values, respectively. (c) Time series of observed and reconstructed precipitation occurrences with 95% predictive interval.

of wet conditions than the average magnitude of extreme precipitation across events. Importantly, however, ARs tend to leave specific spatial signatures of moisture distributed across the coast and Intermountain West and the spatial patterns among growth anomalies in a large network of tree ring chronologies show great promise for being able to reconstruct these extreme events.

4. Conclusion

This work showed for the first time that a network of tree ring chronologies across the West Coast and the Intermountain West can be used to reconstruct the occurrence of AR storm tracks and associated extreme precipitation in that region. In the Southwest, these chronologies record the footprint of cold-season moisture associated with the two primary AR storm tracks that influence the region as they pass through the Peninsular and Sierra Nevada ranges into the interior of the Unites States along preferred, filamentary pathways. The southwestern Unites States focus was motivated by the availability of a gridded, tree ring-based moisture product that is able to isolate cold-season precipitation in that region. Future work will attempt to extend the reconstruction of AR landfalls and extreme precipitation to other regions along the North American west coast, such as the Pacific Northwest. In that region, conduits of low elevation in the Cascades steer ARs deep into the Intermountain West through eastern Oregon and along the Snake River plain into the northern Rocky Mountains of central Idaho and western Montana (Alexander et al., 2015; Rutz et al., 2014, 2015). Tree ring chronologies along this path, particularly at the terminus in Idaho and Montana, could be used to reconstruct occurrences of this northern AR trajectory. Recent efforts toward this end have shown promise (Wise & Dannenberg, 2017). However, larger summer precipitation totals and lower evaporation rates in the Pacific Northwest will require additional care in isolating the wintertime signal, which is becoming increasingly possible by using earlywood and latewood chronologies (Crawford et al., 2015).

If AR landfall occurrences and associated extreme precipitation for different latitudinal bands of western North America can be successfully reconstructed from the network of tree ring chronologies across the coast and Intermountain West, then the potential exists to combine these reconstructions into an integrated framework to reconstruct long-term, structured fluctuations in the latitudinal variability of AR activity. The goal would be to infer slowly varying shifts in the organization of atmospheric circulation that steer ARs toward the West Coast, which manifest in the frequency and magnitude of regional extreme precipitation that is

recorded by the chronologies across the coast and Intermountain West in preferred spatial patterns. There could be a mixture of AR landfalls across different latitudinal bands in any given year, but it is likely that the large-scale circulation leads to a preferred subset of storm patterns with similar orientation contributing to extremes in a given year. The organization in this process could be explored formally using a latent variable model as a unifying statistical framework, where slowly varying components of the climate system could be modeled as a latent (i.e., unobservable) process with smooth fluctuations that can be inferred from noisier fluctuations in modes of extreme precipitation, cold-season chronologies, and AR occurrences. The latent process can be extended backward in time based on the long tree ring based field and can then be subsequently used to reconstruct extreme regional precipitation risk and AR landfall occurrences with the appropriate degree of uncertainty. This effort is left for future work.

References

Alexander, M. A., Scott, J. D., Swales, D., Hughes, M., Mahoney, K., & Smith, C. A. (2015). Moisture pathways into the U.S. Intermountain West associated with heavy winter precipitation events. *Journal of Hydrometeorology*, *16*(3), 1184–1206. https://doi.org/10.1175/JHM-D-14-0139.1

Brands, S., Gutiérrez, J. M., & San-Martín, D. (2017). Twentieth-century atmospheric river activity along the west coasts of Europe and North America: algorithm formulation, reanalysis uncertainty and links to atmospheric circulation patterns. *Climate Dynamics*, *48*, 2771–2795. https://doi.org/10.1007/s00382-016-3095-6

Compo, G. P., Whitaker, J. S., Sardeshmukh, P. D., Matsui, N., Allan, R. J., Yin, X., et al. (2011). The twentieth century reanalysis project. *Quarterly Journal of the Royal Meteorological Society*, *137*(654, A), 1–28. https://doi.org/10.1002/qj.776

Cook, B. I., Smerdon, J. E., Seager, R., & Cook, E. R. (2014). Pan-continental droughts in North America over the last millennium. *Journal of Climate*, *27*(1), 383–397.

Cook, E. R., Meko, D. M., Stahle, D. W., & Cleaveland, M. K. (1999). Drought reconstructions for the continental United States. *Journal of Climate*, *12*(4), 1145–1162. https://doi.org/10.1175/1520-0442(1999)012<1145:DRFTCU>2.0.CO;2

Cook, E. R., Seager, R., Heim, R. R., Vose, R. S., Herweijer, C., & Woodhouse, C. (2010). Megadroughts in North America: Placing IPCC projections of hydroclimatic change in a long-term paleoclimate context. *Journal of Quaternary Science*, *25*(1), 48–61. https://doi.org/10.1002/jqs.1303

Crawford, C. J., Griffin, D., & Kipfmueller, K. F. (2015). Capturing season- specific precipitation signals in the northern Rocky Mountains, USA, using earlywood and latewood tree rings. *Journal of Geophysical Research: Biogeosciences*, *120*, 428–440. https://doi.org/10.1002/2014JG002740

Dee, D. P., Uppala, S. M., Simmons, A. J., Berrisford, P., Poli, P., Kobayashi, S., et al. (2011). The ERA-interim reanalysis: Configuration and performance of the data assimilation system. *Quarterly Journal of the Royal Meteorological Society*, *137*(656), 553–597. https://doi.org/10.1002/qj.828

Demaria, E. M. C., Dominguez, F., Hu, H., von Glinski, G., Robles, M., Skindlov, J., & Walter, J. (2017). Observed hydrologic impacts of landfalling atmospheric rivers in the Salt and Verde river basins of Arizona, United States. *Water Resources Research*, *53*, 10,025–10,042. https://doi.org/10.1002/2017WR020778

Dettinger, M. D. (2004). Fifty-two years of Pineapple-Express Storms across the West Coast of North America. California Energy Commission PIER Energy-Related Environmental Research Report CEC-500-2005-004, Sacramento, California, 15 pp.

Dettinger, M. D. (2013). Atmospheric rivers as drought busters on the U.S. west coast. *Journal of Hydrometeorology*, *14*(6), 1721–1732. https://doi.org/10.1175/JHM-D-13-02.1

Dettinger, M. D., Ralph, F. M., Das, T., Neiman, P. J., & Cayan, D. R. (2011). Atmospheric rivers, floods, and the water resources of California. *Water*, *2011*(3), 445–478. https://doi.org/10.3390/w3020445

Dobyns, H. R. (1981). *From fire to flood: Historic human destruction of Sonoran desert riverine oases* (p. 222). Socorro, New Mexico: Ballena Press.

Guan, B., Molotch, N. P., Waliser, D. E., Fetzer, E. J., & Neiman, P. J. (2010). Extreme snowfall events linked to atmospheric rivers and surface air temperature via satellite measurements. *Geophysical Research Letters*, *37*, L20401. https://doi.org/10.1029/2010GL044696

Hughes, M., Mahoney, K. M., Neiman, P. J., Moore, B. J., Alexander, M., & Ralph, F. M. (2014). The landfall and inland penetration of a flood-producing atmospheric river in Arizona. Part II: Sensitivity of modeled precipitation to terrain height and atmospheric river orientation. *Journal of Hydrometeorology*, *15*(5), 1954–1974. https://doi.org/10.1175/JHM-D-13-0176.1

Kalnay, E., Kanamitsu, M., Kistler, R., Collins, W., Deaven, D., Gandin, L., et al. (1996). The NCEP/NCAR 40-Year Reanalysis Project. *Bulletin of the American Meteorological Society*, *77*(3), 437–471. https://doi.org/10.1175/1520-0477(1996)077<0437:TNYRP>2.0.CO;2

Livneh, B., Rosenberg, E. A., Lin, C., Nijssen, B., Mishra, V., Andreadis, K. M., et al. (2013). A long-term hydrologically based dataset of land surface fluxes and states for the conterminous United States: Update and extensions. *Journal of Climate*, *26*(23), 9384–9392. https://doi.org/10.1175/JCLI-D-12-00508.1

Meko, D. M., Stahle, D. W., Griffin, D., & Knight, T. A. (2011). Inferring precipitation-anomaly gradients from tree-rings. *Quaternary International*, *235*(1–2), 89–100. https://doi.org/10.1016/j.quaint.2010.09.006

Neiman, P. J., Ralph, F. M., Moore, B. J., Hughes, M., Mahoney, K. M., Cordeira, J. M., & Dettinger, M. D. (2013). The landfall and inland penetration of a flood-producing atmospheric river in Arizona. Part I: Observed synoptic-scale, orographic, and hydrometeorological characteristics. *Journal of Hydrometeorology*, *14*(2), 460–484. https://doi.org/10.1175/JHM-D-12-0101.1

Paulson, R.W., Chase, E. B., Roberts, R. S., & Moody, D. W. (1989), Compilers, National Water Summary 1988–89—Hydrologic events and floods and droughts: U.S. Geological Survey Water-Supply Paper 2375, 591 pp.

Poli, P., Hersbach, H., Tan, D., Dee, D., Thépaut, J. N., Simmons, A., et al. (2013). The data assimilation system and initial performance evaluation of the ECMWF pilot reanalysis of the 20th-century assimilating surface observations only (ERA-20C). Technical report, ERA report series 14.

Ralph, F. M., Neiman, P. J., Wick, G. A., Gutman, S. I., Dettinger, M. D., Cayan, D. R., & White, A. B. (2006). Flooding on California's Russian River: Role of atmospheric rivers. *Geophysical Research Letters*, *33*, L13801. https://doi.org/10.1029/2006GL026689

Rivera, E. R., Dominguez, F., & Castro, C. L. (2014). Atmospheric rivers and cool season extreme precipitation events in the Verde River Basin of Arizona. *Journal of Hydrometeorology*, *15*(2), 813–829. https://doi.org/10.1175/JHM-D-12-0189.1

Rutz, J. J., & Steenburgh, W. J. (2012). Quantifying the role of atmospheric rivers in the interior western United States. *Atmospheric Science Letters*, *13*(4), 257–261. https://doi.org/10.1002/asl.392

Rutz, J. J., Steenburgh, W. J., & Ralph, F. M. (2014). Climatological characteristics of atmospheric rivers and their inland penetration over the western United States. *Monthly Weather Review*, *142*(2), 905–921. https://doi.org/10.1175/MWR-D-13-00168.1

Rutz, J. J., Steenburgh, W. J., & Ralph, F. M. (2015). The inland penetration of atmospheric rivers over western North America: A Lagrangian analysis. *Monthly Weather Review*, *143*(5), 1924–1944. https://doi.org/10.1175/MWR-D-14-00288.1

Steinschneider, S., Ho, M., Cook, E. R., & Lall, U. (2016). Can PDSI inform extreme precipitation?: An exploration with a 500 year long paleo-climate reconstruction over the U.S. *Water Resources Research*, *52*, 3866–3880. https://doi.org/10.1002/2016WR018712

St. George, S., & Ault, T. R. (2014). The imprint of climate within Northern Hemisphere trees. *Quaternary Science Reviews*, *89*, 1–4. https://doi.org/10.1016/j.quascirev.2014.04.029

St. George, S., Meko, D. M., & Cook, E. R. (2010). The seasonality of precipitation signals embedded within the North American Drought Atlas. *Holocene*, *20*(6), 983–988. https://doi.org/10.1177/0959683610365937

Swales, D., Alexander, M., & Hughes, M. (2016). Examining moisture pathways and extreme precipitation in the U.S. Intermountain West using self-organizing maps. *Geophysical Research Letters*, *43*, 1727–1735. https://doi.org/10.1002/2015GL067478

Torbenson, M. C. A. (2018). Cool and warm season climate signals in tree rings from the Americas, (PhD Dissertation). Dept. of Geosciences, University of Arkansas, Fayetteville, 180 pp.

Williams, A. P., Michaelsen, J., Leavitt, S. W., & Still, C. J. (2010). Using tree-rings to predict the response of tree growth to climate change in the continental United States during the 21st century. *Earth Interactions*, *14*(19), 1–20. https://doi.org/10.1175/2010EI362.1

Wise, E. K., & Dannenberg, M. P. (2014). Persistence of pressure patterns over North America and the North Pacific since AD 1500. *Nature Communications*, *5*(1), 4912. https://doi.org/10.1038/ncomms5912

Wise, E. K., & Dannenberg, M. P. (2017). Reconstructed storm tracks reveal three centuries of changing moisture delivery to North America. *Science Advances*, *3*(6), e1602263. https://doi.org/10.1126/sciadv.1602263

Woodhouse, C. A., & Meko, D. M. (1997). Number of winter precipitation days reconstructed from southwestern tree rings. *Journal of Climate*, *10*(10), 2663–2669. https://doi.org/10.1175/1520-0442(1997)010<2663:NOWPDR>2.0.CO;2

Zhu, Y., & Newell, R. E. (1994). Atmospheric rivers and bombs. *Geophysical Research Letters*, *21*(18), 1999–2002. https://doi.org/10.1029/94GL01710